Dielectric Discontinuity at Interfaces in the Atomic-Scale Limit: Permittivity of Ultrathin Oxide Films on Silicon

Feliciano Giustino, Paolo Umari, and Alfredo Pasquarello

Institut de Théorie des Phénomènes Physiques (ITP), Ecole Polytechnique Fédérale de Lausanne (EPFL), CH-1015 Lausanne, Switzerland

Institut Romand de Recherche Numérique en Physique des Matériaux (IRRMA), CH-1015 Lausanne, Switzerland

(Received 7 July 2003; published 24 December 2003)

Using a density-functional approach, we study the dielectric permittivity across interfaces at the atomic scale. Focusing on the static and high-frequency permittivities of SiO_2 films on silicon, for oxide thicknesses from 12 Å down to the atomic scale, we find a departure from bulk values in accord with experiment. A classical three-layer model accounts for the calculated permittivities and is supported by the microscopic polarization profile across the interface. The local screening varies on length scales corresponding to first-neighbor distances, indicating that the dielectric transition is governed by the chemical grading. Silicon-induced gap states are shown to play a minor role.

DOI: 10.1103/PhysRevLett.91.267601 PACS numbers: 77.55.+f, 73.61.–r, 71.15.–m

In the macroscopic regime, the permittivity of two adjacent dielectrics is obtained from those of the respective bulk materials according to classical electrostatics. However, when the thickness of one component approaches the atomic scale, the resulting permittivity can be obtained only through a detailed quantum mechanical description of the electronic structure [1]. Understanding the dielectric screening in the vicinity of interfaces is generally of great practical relevance in thin film metrology. Indeed, the extraction of film thicknesses from both ellipsometric [2] and capacitance-voltage [3] measurements relies on *ad hoc* models of the dielectric response. More recently, the dielectric permittivity of ultrathin SiO_2 films has acquired importance in the context of silicon technology. While current research is focusing on the replacement of the gate oxide SiO_2 by a material of higher dielectric permittivity κ [4], the undesired formation of an ultrathin SiO_2 interlayer could compromise the overall permittivity of the gate dielectric [5]. However, recent observations suggest that the permittivity of such an interlayer is appreciably higher than that of bulk SiO_2 [6,7].

In this work, we introduce a scheme within density-functional theory to address dielectric discontinuities at interfaces. We focus here on the Si-SiO_2 interface because of its immediate interest in silicon technology. Using atomistic structures, we calculate both the static (ϵ_0) and high-frequency (ϵ_∞) dielectric permittivities of ultrathin SiO_2 films on silicon, for oxide thicknesses up to 12 Å. First, we show that the calculated permittivities are accurately reproduced by a classical three-layer model. We then rationalize this finding by determining the microscopic polarization profile across the interface. An analysis of the local screening based on the Berry-phase theory of polarization reveals that the dielectric transition is dominated by the chemical grading. Induced gap states are shown to play a minor role.

The electronic structure is described within a generalized gradient approximation to density-functional theory [8]. We used a normconserving pseudopotential for Si atoms [9] and an ultrasoft pseudopotential for O atoms [10]. The valence electron wave functions and the augmented charge density were described by plane-wave basis sets with energy cutoffs of 24 and 150 Ry, respectively [11]. The Brillouin zones of our systems were sampled at the Γ point. All our model structures were fully relaxed by means of a damped molecular dynamics scheme [11,12]. We obtained ϵ_0 and ϵ_∞ by evaluating the variation of the polarization in response to a *finite* electric field, thereby avoiding the determination of the dynamical matrix [13].

To model the interface between silicon and its oxide we used -Si-SiO_2- superlattices. The simulation cell contains two -Si-SiO_2- interfaces connected back-to-back, which carry by symmetry the same permittivities as the full superlattice. We used an interface bonding pattern in which a β-cristobalite oxide structure is matched without coordination defects to Si(100), as described in Ref. [14]. At the transition from silicon to SiO_2, the three intermediate oxidation states of Si, Si^{+1}, Si^{+2}, and Si^{+3}, occur in equal amounts of 0.5 ML and are distributed over two atomic layers, in qualitative agreement with recent photoemission experiments [15]. The choice of β cristobalite allows us to vary the oxide thickness by steps as small as one molecular layer (~2 Å).

We constructed six superlattices with 11 Si monolayers (≃15 Å) and up to 10 SiO_2 molecular layers (≃17 Å) in the direction orthogonal to the interface planes (x direction). In the plane of the interface, we used a fixed 2×2 interface Si unit with supercell parameters $L_y = L_z = 7.75$ Å, based on the theoretical lattice constant. To determine the supercell parameter in the x direction L_x, we performed a separate relaxation of the interface model with 10 SiO_2 molecular layers in a slab geometry, using H atoms to

saturate the free surfaces. Beyond one molecular layer from the interface, the structural parameters were found to deviate negligibly from those of bulk SiO_2 (i.e., Si-matched β-cristobalite [16]).

To focus on the role of the oxide overlayer, it is convenient to analyze the calculated permittivities in terms of contributions from two distinct dielectrics: the oxide overlayer and the Si substrate. We obtained the permittivity of the oxide overlayer ($\epsilon_{\rm overl}$) by removing the contribution of the latter on the basis of classical electrostatics. This required the thickness and the permittivity of the substrate component, which were derived from the amount of nonoxidized Si atoms and from separate bulk calculations [17,18], respectively. Figure 1 shows that both the static and high-frequency permittivities of the oxide overlayer significantly increase with decreasing thickness. For the thinnest overlayer, the permittivities are almost twice as large as those of bulk SiO_2 ($\epsilon_{\rm ox}^0 = 3.8$ and $\epsilon_{\rm ox}^\infty = 2.0$) [19]. For increasing thicknesses, the permittivities decay algebraically to the bulk SiO_2 values. We note that both the electronic and the ionic screening contribute to the observed enhancement of the permittivity (Fig. 1, inset). These results indicate that the first few atomic layers of the oxide near the substrate exhibit dielectric properties significantly different from bulk SiO_2, in accord with recent experimental observations [6]. This effect is at the origin of the overestimation of the film thickness when determined by ellipsometry [7]. A further important implication for high-κ gate dielectrics on silicon is that the capacitance reduction due to a thin SiO_2 interlayer is less severe than expected [5].

The behavior of the permittivities in Fig. 1 demonstrates that a classical picture based on two dielectrics is inconsistent with the data in a regime of atomic-layer thicknesses. We then investigated whether a classical description can be recovered at the cost of introducing a third intermediate dielectric. For this purpose, we modeled the permittivity of the oxide overlayer ($\epsilon_{\rm overl}^{\rm mod}$) by considering two dielectrics, bulk SiO_2 and a thin suboxide layer. Classical electrostatics then gives

$$\epsilon_{\rm overl}^{\rm mod} = t_{\rm overl}\left(\frac{t_{\rm ox}}{\epsilon_{\rm ox}} + \frac{t_{\rm sub}}{\epsilon_{\rm sub}}\right)^{-1}, \tag{1}$$

where the thickness $t_{\rm ox}$ of the SiO_2 component is derived from the number of fully oxidized Si atoms and the density of bulk SiO_2. The thickness of the suboxide layer ($t_{\rm sub} = 3.2$ Å) is then obtained as a difference. As an estimate of the suboxide permittivity $\epsilon_{\rm sub}$, we took $\epsilon_{\rm overl}$ corresponding to the superlattice without any fully oxidized Si atom ($\epsilon_{\rm sub}^\infty = 3.8$, $\epsilon_{\rm sub}^0 = 7.1$). For oxide thicknesses up to 12 Å, $\epsilon_{\rm overl}^{\rm mod}$ given by Eq. (1) agrees with $\epsilon_{\rm overl}$ calculated in the density-functional approach within 2% (Fig. 1). Hence, it is possible to *classically* account for the dielectric properties of the Si-SiO_2 interface down to the atomic scale.

To understand why such a classical description holds, we analyzed the *microscopic* response to an electric field along the x axis. From the in-medium Maxwell equation $\nabla \cdot \mathbf{p}(\mathbf{r}) = -\rho_{\rm ind}(\mathbf{r})$ [20], we obtain a relation between the induced microscopic polarization along x, $\overline{p}_x(x)$, and the induced charge density, $\overline{\rho}_{\rm ind}(x)$:

$$\frac{\partial}{\partial x}\overline{p}_x(x) = -\overline{\rho}_{\rm ind}(x), \tag{2}$$

where the bars indicate averages over the yz directions. Note that, unlike the microscopic polarization $\mathbf{p}(\mathbf{r})$, its planar average $\overline{p}_x(x)$ is gauge invariant. In this work, we evaluated the induced charge density $\overline{\rho}_{\rm ind}$ by applying finite electric fields [13] in the linear regime and taking finite differences of the resulting charge densities. Equation (2) then gives $\overline{p}_x(x)$ up to an additive constant, which is determined by the overall Berry-phase polarization induced in the supercell [21]. For illustration, we focused on the response of the superlattice with an oxide thickness of 24 Å. We calculated both the high-frequency and the static microscopic polarization across the interface (Fig. 2). For the static polarization, we used Gaussian distributions to represent the ionic point charges. The microscopic polarizations remain constant in the silicon bulk region, decrease continuously through the suboxide, and reassume constant values in the oxide. In both the static and high-frequency regimes, the classical three-layer model describes this behavior by a three-step approximation to the polarization, in which the intermediate value closely corresponds to the average microscopic one in the suboxide region. The accord with the classical model supports the notion that the dielectric transition from Si to SiO_2 is rather abrupt, and essentially takes place within the suboxide region. This picture is also consistent with very recent Auger measurements showing that the oxide permittivity beyond 6 Å from the interface agrees with that of bulk SiO_2 [22].

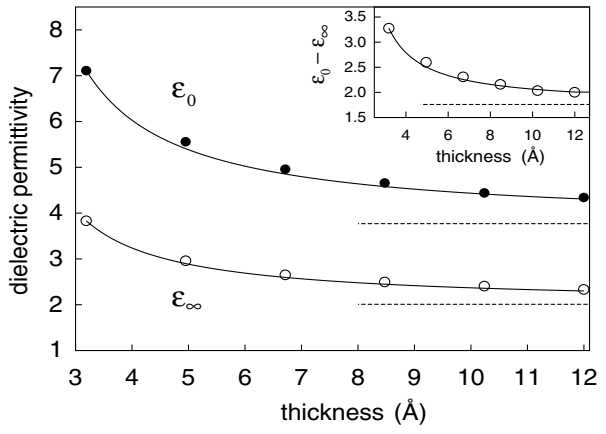

FIG. 1. Permittivities ϵ_∞ (circles) and ϵ_0 (disks) of the oxide overlayer vs its thickness, compared to the results of a classical three-layer model (solid). The classical two-layer model gives a constant permittivity corresponding to that of bulk SiO_2 (dashed). Inset: ionic contribution to ϵ_0.

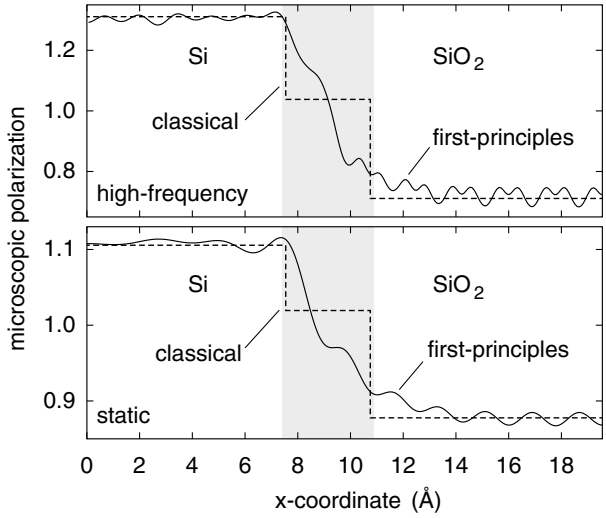

FIG. 2. High-frequency (upper panel) and static (lower panel) microscopic polarization along x (solid lines) compared to the classical three-layer model (dashed lines). The polarization is normalized by its average value in the cell. For the static polarization we used a Gaussian broadening of 0.9 Å to smear out the pointlike ionic contributions. The suboxide region is shaded.

To understand the variation of the microscopic polarization across the dielectric transition layer, we introduce appropriate polarizable units and determine their *effective* polarizabilities. For this purpose, we chose Si-centered structural units including eventual nearest neighbor O atoms. For each polarizable unit, we defined an effective induced electric field as a suitable average of the microscopic induced field over the polarizable unit. To assign an induced electronic dipole to each polarizable unit, it is convenient to describe the electronic structure in terms of Wannier functions w_n, maximally localized along the x axis [23]. Following the modern theory of polarization [21], the electronic polarization is given in terms of the displacements Δx_n of the Wannier functions induced by the electric field:

$$P_x^{\mathrm{el}} = \frac{2e}{\Omega}\sum_n \Delta x_n = \frac{2e}{\Omega}\sum_n \Delta\langle w_n|x|w_n\rangle, \qquad (3)$$

where e is the electron charge, and Ω the volume of our cell. Thus, we can attribute an induced dipole to each Wannier function. Since each Wannier function can be associated either to a structural bond or to a nonbonding O orbital, it is straightforward to define the induced dipole of a polarizable unit, and, consequently, its electronic polarizability by means of the effective field. The resulting polarizabilities are shown in Fig. 3 (upper panel). These polarizabilities are found to vary with the oxidation state of the central Si atom, decreasing from Si^0 to Si^{+4}.

A similar analysis can be carried out for the ionic contribution to the polarization. In the linear regime, the latter is given by [24]

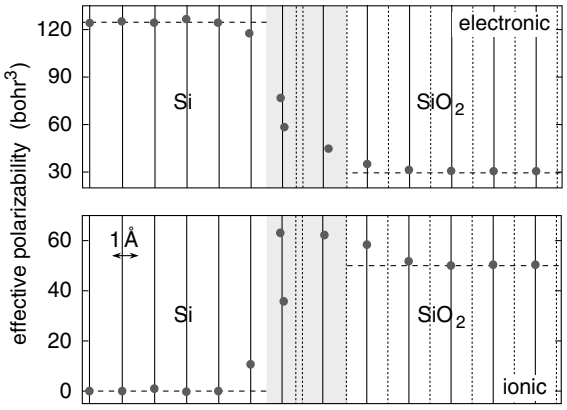

FIG. 3. Electronic (upper panel) and ionic (lower panel) polarizability of the Si-centered polarizable units defined in the text vs their position along the x axis. The Si and SiO_2 bulk values are shown (dashed lines). Vertical lines represent planes of Si (solid lines) and O atoms (dashed lines). The suboxide region is shaded.

$$P_x^{\mathrm{ion}} = \frac{1}{\Omega}\sum_{I\alpha} Z^*_{I,x\alpha} u_{I,\alpha}, \qquad (4)$$

where $Z^*_{I,x\alpha}$ are the transverse dynamical charges [25], $u_{I,\alpha}$ the ionic displacements, α runs over the Cartesian directions, and I over the atoms. In our finite-field scheme, the displacements $u_{I,\alpha}$ are obtained by relaxation and the dynamical charges $Z^*_{I,x\alpha}$ from the atomic forces [13]. From the atomic contributions in Eq. (4), we determined the induced dipoles of the polarizable units. The ionic polarizabilities then follow via the effective field [Fig. 3 (lower panel)] [26]. These polarizabilities vanish in the silicon region (because of the vanishing dynamical charges) and reach the bulk SiO_2 value on the oxide side. In the suboxide region, the polarizabilities are larger than in SiO_2, in accord with the classical model. The present analysis of both the electronic and the ionic screening reveals that the dielectric transition across the interface strongly relates to the grading of the chemical composition. This is consistent with ellipsometric data for Si-SiO_2 interfaces with broader transition layers [2].

At variance with our findings, the dielectric transition at Si-SiO_2 interfaces has previously been related to the tails of Si states at energies located inside the SiO_2 band gap [5,27], in analogy to the metal induced gap states at metal-semiconductor contacts [28]. These tails extend into the oxide for about 5 Å contributing to a reduction of the gap in the local density of states [27,29]. To investigate the role of such tails, we retain for each Wannier function a fraction of its contribution to the microscopic polarization, corresponding to its projection onto the occupied electronic states lying inside the oxide gap. Figure 4 shows that the combination of these contributions decays into the oxide on a similar length scale as the formation of the oxide gap. In the near-interface oxide (first 5 Å), the contribution from gap states amounts to only 13% of the polarization [30], indicating that their

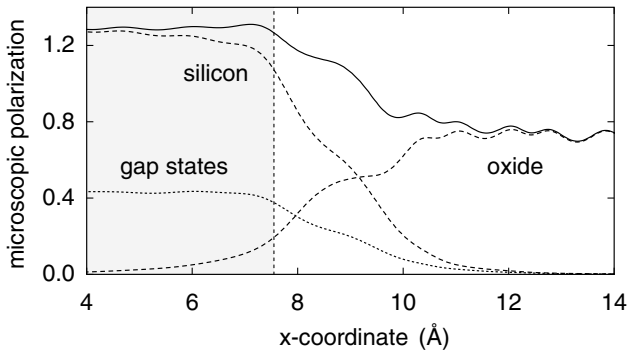

FIG. 4. Microscopic electronic polarization [solid, from Fig. 2 (upper panel)] and the contribution from gap states (dots). The shaded area corresponds to the Si layer. For comparison, we also show a decomposition in silicon and oxide contributions on the basis of localized Wannier functions (dashed): the silicon contribution results from Si-Si bonds, the oxide one from Si-O bonds and O nonbonding orbitals.

role is secondary. This assertion is further supported by considering the Schottky pinning factor of SiO_2, which can be related to the screening due to gap states [31–33]. We derived an estimate of 0.8 for this Schottky pinning factor, in accord with experimental data (0.70–0.86) [31].

In conclusion, we investigated the dielectric transition across the Si-SiO_2 interface at the atomic scale. For atomic-layer thin films (3–5 Å), we observed a significant enhancement of the oxide permittivity. This has important implications for the gate capacitance of high-κ dielectrics on silicon in the presence of SiO_2 interlayers. More generally, this work defines a comprehensive scheme for addressing dielectric discontinuities across interfaces in a systematic way.

We thank A. Baldereschi for fruitful discussions. Support is acknowledged from the Swiss National Science Foundation (Grant No. 620-57850.99) and the Swiss Center for Scientific Computing.

[1] J. R. Jameson, W. Harrison, and P. B. Griffin, J. Appl. Phys. **92**, 4431 (2002).
[2] D. E. Aspnes and J. B. Theeten, Phys. Rev. Lett. **43**, 1046 (1979).
[3] B. Brar, G. D. Wilk, and A. C. Seabaugh, Appl. Phys. Lett. **69**, 2728 (1996).
[4] G. D. Wilk, R. M. Wallace, and J. M. Anthony, J. Appl. Phys. **89**, 5243 (2001).
[5] D. A. Muller and G. D. Wilk, Appl. Phys. Lett. **79**, 4195 (2001).
[6] C. M. Perkins *et al.*, Appl. Phys. Lett. **78**, 2357 (2001).
[7] H. S. Chang *et al.*, J. Vac. Sci. Technol. B **20**, 1836 (2002).
[8] J. P. Perdew and Y. Wang, Phys. Rev. B **46**, 12 947 (1992).
[9] A. Dal Corso, A. Pasquarello, A. Baldereschi, and R. Car, Phys. Rev. B **53**, 1180 (1996).
[10] D. Vanderbilt, Phys. Rev. B **41**, 7892 (1990).
[11] A. Pasquarello *et al.*, Phys. Rev. Lett. **69**, 1982 (1992); K. Laasonen *et al.*, Phys. Rev. B **47**, 10 142 (1993).
[12] R. Car and M. Parrinello, Phys. Rev. Lett. **55**, 2471 (1985).
[13] P. Umari and A. Pasquarello, Phys. Rev. Lett. **89**, 157602 (2002).
[14] A. Pasquarello, M. S. Hybertsen, and R. Car, Phys. Rev. B **53**, 10 942 (1996); Appl. Surf. Sci. **104**, 317 (1996).
[15] F. Rochet *et al.*, J. Non-Cryst. Solids **216**, 148 (1997); J. H. Oh *et al.*, Phys. Rev. B **63**, 205310 (2001).
[16] The oxide is characterized by a Si-O bond length of 1.63 Å, O-Si-O angles within a few percent from the ideal tetrahedral value, and Si-O-Si angles close to 180°.
[17] Using supercells with the same cell parameters L_y and L_z as the superlattices, we obtained permittivity values for bulk Si (ϵ_{Si}) between 12.2 and 13.6, for cell parameters L_x varying in the range of those of the superlattices. This dependence results from the Γ-point sampling and is effectively removed in Fig. 1 by taking values of ϵ_{Si} pertaining to the same L_x as the corresponding superlattice.
[18] We accounted for the effect of quantum confinement by evaluating ϵ_{Si} from the local polarizability of the deepest Si layers in the superlattices (cf. text). This effect reduces the bulk ϵ_{Si} by $8 \pm 1\%$.
[19] We obtained permittivities for β-cristobalite matched to silicon from separate calculations. The dependence on the parameter L_x of the superlattice is negligible.
[20] L. L. Hirst, Rev. Mod. Phys. **69**, 607 (1997).
[21] R. D. King-Smith and D. Vanderbilt, Phys. Rev. B **47**, 1651 (1993); R. Resta, Rev. Mod. Phys. **66**, 899 (1994).
[22] K. Hirose, H. Kitahara, and T. Hattori, Phys. Rev. B **67**, 195313 (2003).
[23] N. Marzari and D. Vanderbilt, Phys. Rev. B **56**, 12 847 (1997); C. Sgiarovello, M. Peressi, and R. Resta, Phys. Rev. B **64**, 115202 (2001); we used the method proposed in F. Gygi, J.-L. Fattebert, and E. Schwegler, Comput. Phys. Commun. **155**, 1 (2003).
[24] A. A. Maradudin, E. W. Montroll, G. H. Weiss, and I. P. Ipatova, *Theory of Lattice Dynamics in the Harmonic Approximation*, Solid State Physics Suppl. 3 (Academic, New York, 1971).
[25] Ph. Ghosez, J.-P. Michenaud, and X. Gonze, Phys. Rev. B **58**, 6224 (1998).
[26] To ensure the local nature of the ionic polarizabilities, we derived the $Z^*_{I,x\alpha}$ using the effective field rather than the macroscopic one.
[27] D. A. Muller *et al.*, Nature (London) **399**, 758 (1999); J. B. Neaton, D. A. Muller, and N. W. Ashcroft, Phys. Rev. Lett. **85**, 1298 (2000).
[28] J. Bardeen, Phys. Rev. **71**, 717 (1947); V. Heine, Phys. Rev. **138**, A1689 (1965); A. M. Cowley and S. M. Sze, J. Appl. Phys. **36**, 3212 (1965).
[29] T. Yamasaki, *et al.*, Phys. Rev. B **63**, 115314 (2001).
[30] From Fig. 1 and the percentage of 13%, we derived an effective susceptibility of gap states: $4\pi\chi_{gs} \simeq 0.3$.
[31] W. Mönch, Surf. Sci. **299**, 928 (1994).
[32] J. Robertson, J. Vac. Sci. Technol. B **18**, 1785 (2000).
[33] C. Berthod, N. Binggeli, and A. Baldereschi, Europhys. Lett. **36**, 67 (1996).